APPLIED AND ENVIRONMENTAL MICROBIOLOGY, Mar. 1995, p. 926–936 Vol. 61, No. 3
0099-2240/95/$04.00+0

Fully Automatic Determination of Soil Bacterium Numbers, Cell Volumes, and Frequencies of Dividing Cells by Confocal Laser Scanning Microscopy and Image Analysis

JAAP BLOEM,[1]* MEINT VENINGA,[1] AND JOHN SHEPHERD[2]

DLO-Research Institute for Agrobiology and Soil Fertility, NL-9750 AC Haren, The Netherlands,[1] *and Leica Cambridge Ltd., Cambridge CB1 3QH, England*[2]

Received 22 July 1994/Accepted 17 November 1994

We describe a fully automatic image analysis system capable of measuring cell numbers, volumes, lengths, and widths of bacteria in soil smears. The system also determines the number of cells in agglomerates and thus provides the frequency of dividing cells (FDC). Images are acquired from a confocal laser scanning microscope. The grey images are smoothed by convolution and by morphological erosion and dilation to remove noise. The background is equalized by flooding holes in the image and is then subtracted by two top hat transforms. Finally, the grey image is sharpened by delineation, and all particles above a fixed threshold are detected. The number of cells in each detected particle is determined by counting the number of local grey-level maxima in the particle. Thus, up to 1,500 cells in 10 fields of view in a soil smear are analyzed in 30 min without human intervention. Automatic counts of cell numbers and FDC were similar to visual counts in field samples. In microcosms, automatic measurements showed significant increases in cell numbers, FDC, mean cell volume, and length-to-width ratio after amendment of the soil. Volumes of fluorescent microspheres were measured with good approximation, but the absolute values obtained were strongly affected by the settings of the detector sensitivity. Independent measurements of bacterial cell numbers and volumes by image analysis and of cell carbon by a total organic carbon analyzer yielded an average specific carbon content of 200 fg of C μm^{-3}, which indicates that our volume estimates are reasonable.

Microorganisms play a major role in the decomposition of organic matter and the mineralization and immobilization of nitrogen in soil. The development and application of models of carbon and nitrogen cycling in soil ecosystems require reliable quantitative estimates of biomass and activity of the main functional groups of soil organisms, such as bacteria, fungi, protozoa, and nematodes (13, 14). The contribution of bacteria to the total biomass in Dutch agricultural soils has been estimated to be about 80%, whereas fungi were found to contribute 10% or less (7, 19, 32).

Epifluorescence microscopy has become the major technique for direct enumeration of bacteria in aquatic as well as terrestrial ecosystems (17). In principle, a known amount of homogenized soil suspension is placed on a known area of a microscope slide, the microorganisms are stained with a fluorescent dye which binds to proteins or nucleic acids, and numbers are tallied under a microscope with epiillumination by UV or blue light excitation (9). Cell volumes can be estimated from lengths and widths, and the total bacterial biovolume can be estimated from the product of the total count and mean cell volume. The biovolume in turn can be converted to biomass by multiplication with the specific carbon content, which has been estimated to be 310 fg of C μm^{-3} (17). The frequency of dividing cells (FDC), i.e., the percentage of cells showing an invagination, can be used as an index of the in situ specific growth rate of bacteria in water (18) and also in soil (6, 7).

Visual counting of bacterial numbers in field samples can be done reasonably fast but is rather subjective because of the presence of weakly stained, presumably inactive or dead cells which are hard to distinguish from dead organic matter. Estimation of the FDC and of cell lengths and widths, however, is very inaccurate and time-consuming. For aquatic samples, biomass estimates have been greatly improved by the use of computerized image analysis (3, 16, 29). In principle, grey images of 512 by 512 pixels (picture elements) are acquired from a sensitive video camera on an epifluorescence microscope. Each pixel has a size of about 0.1 μm and a grey value between 0 (black) and 255 (white). Since bacteria in the image are represented by bright spots against a dark background, a threshold grey value can be set to segment the grey image into a binary image in which all pixels above the threshold are represented by a value of 1 (particle) and pixels below the threshold are represented by a value of 0 (background). Then the number of particles (presumably bacteria) is counted, and the size of each particle is calculated from the number of pixels it occupies. Bjørnsen (3) described a system that was capable of measuring 250 cells within 10 min, giving estimates of the cell number, mean cell volume, and total biovolume. The systems described (3, 29) were semiautomatic since unwanted detrital particles were removed by interactive editing and thresholds were set visually for each image by the operator.

It has been questioned whether it would be possible to apply image analysis to the measurement of soil bacteria (17). We performed some preliminary measurements of bacteria in soil smears with the system used by Bjørnsen (3) and with the system developed by Schröder and Krambeck (24) for the measurement of bacteria in water samples. Bacteria in soil samples are more difficult to analyze than those in water samples, because only part of the cells are in focus simultaneously as a result of the thickness of the soil film on the microscopic slide and the limited depth of focus of a conventional microscope. Moreover, there is more background staining than in most water samples. Nevertheless, it was possible to measure cell sizes if detrital particles were removed and cells in agglom-

* Corresponding author. Mailing address: AB-DLO, P.O. Box 129, NL-9750 AC Haren, The Netherlands. Phone: 31 50 337354. Fax: 31 50 337291. Electronic mail address: Bloem@ab.agro.nl.

erates were separated manually. The two systems yielded similar estimates of the mean cell volume (6).

Here, we describe an image analysis system capable of measuring numbers, volumes, lengths, and widths of bacteria in soil smears fully automatically, without manual editing and without manually setting a threshold (it is set automatically). The system also determines the number of cells per agglomerate and thus provides the FDC automatically. The problem of the thickness of the soil smear was overcome by using a confocal laser scanning microscope (CLSM), which offers an extended depth of focus, better contrast, and better resolution than a conventional epifluorescence microscope (10, 11). The good contrast and resolution facilitate the detection of individual cells in agglomerates and decrease the problem of background staining.

MATERIALS AND METHODS

Preparation of soil smears. Soil samples were collected from an arable field (field 16A) at the Lovinkhoeve experimental farm (7). The soil is a calcareous silt loam with the following characteristics (0- to 25-cm layer): pH (in a soil suspension with 1 M KCl) of 7.3 to 7.7, 9% $CaCO_3$, 12% sand, 68% silt, 20% clay, 2.8% organic matter, and 0.14% total soil N. At least 15 soil cores (diameter, 3.5 cm) were bulked in a plastic bag and mixed by hand.

For each sample, 20 g of soil and 190 ml of demineralized and filter-sterilized water were homogenized in a blender (Waring, New Hartford, Conn.) for 1 min at maximum speed (20,000 rpm) (5). A 9-ml sample of the soil suspension was fixed by adding 1 ml of formaldehyde (final concentration, 3.7%). The fixed soil suspension was resuspended on a Vortex test tube mixer. After 2 min of settling to remove coarse particles, 10 μl of soil suspension (0.9 mg of soil) was evenly smeared in a circle with a diameter of 12 mm on a microscope slide (2). Before use, the slides were precleaned with 70% ethanol to remove hydrophobic material from the glass surface and were then sealed with pieces of self-adhesive tape (4 by 2 cm) with a hole (12 mm in diameter) punched in the center. The plastic tape (4 cm wide, Boeklon foil no. 27110; Nederlands Bibliotheek en Lektuur Centrum, The Hague, The Netherlands) is normally used to cover books. The water-repellent tape keeps the soil suspension in a defined area of 113 mm^2. The slides were air dried, the tape was peeled off, and the spots of dried soil film were flooded with drops of stain solution for 30 min at room temperature. The stain solution consisted of 2 mg of 5-(4,6-dichlorotriazin-2-yl)aminofluorescein (DTAF) dissolved in 10 ml of phosphate buffer (0.05 M Na_2HPO_4 with 0.85% NaCl [pH 9]) (27). The stain solution was not stored for longer than 1 day. DTAF is a protein stain which has binding, absorption, and emission properties nearly identical to those of fluorescein isothiocyanate. It is superior to fluorescein isothiocyanate with regard to purity and stability (4). We did not use fluorescein isothiocyanate (2), because staining sometimes failed for unknown reasons. After staining, the slides were rinsed three times for 20 min each with phosphate buffer (pH 9) and finally for a few seconds with water by putting them in slide holders and passing them through four baths. The slides were air dried, a coverslip was mounted with immersion oil, and the edges were sealed with nail polish. The slides were stored at 2°C until observation. After 1 year of storage, no deterioration was observed (5).

CLSM. Video images of the slides were generated by a CLSM (Leica Laser Technik GmbH, Heidelberg, Germany), in which the specimen is excited with a scanning laser beam that produces a point source of light in the object plane. The resulting fluorescence from the stained microorganisms is detected by (one or more) sensitive photomultipliers. The intensity of the fluorescent light is recorded as a pixel grey value, ranging from 0 to 255, in an image store. A complete video image is produced by moving the light point over the entire image field line by line. Each line was averaged at least four times to improve the signal-to-noise ratio. Because of the confocal principle, during scanning only light from a very small volume of the specimen (which is in focus) reaches the detector. Stray light from surrounding parts of the specimen (which are not in focus) is blocked by a pinhole in front of the detectors. The size of the pinhole, and thus the confocal effect (i.e., the sampled volume), can be varied. This produces sharp images of thin slices of the specimen (0.5 μm thick) with very good contrast. Usually, nine subsequent slices were scanned in each field of view and stored in the image planes of the CLSM host computer (MC 68020/68881, 20 MHz, 4-Mb RAM and 2-Mb frame memory, 50-Mb hard disk, 800-Mb optical disk). Then the computer calculated a projection of all stored planes and constructed one final image of 50 by 50 μm (512 by 512 pixels) with all bacteria from the total 4.5-μm-thick layer in focus. The projection was based on the maximum grey level found in the subsequent slices. This scanning and imaging procedure is carried out by a macro (short program) on the CLSM computer and takes 90 s. Usually, a pixel size of 0.098 μm was used. The magnification can be increased by zooming the scanning laser beam on a smaller area of the object. Thus, by doubling the zoom factor, an area of 25 by 25 μm is imaged by 512 by 512 pixels, resulting in a pixel size of 0.049 μm.

The differences between an image from a conventional epifluorescence microscope and a confocal image from the CLSM are illustrated in Fig. 1. The conventional image of the DTAF-stained soil bacteria, made by microphotography with Kodak Ektachrome 100 ASA film, shows that only part of the cells are in focus because of the thickness of the soil smear (Fig. 1a). A confocal image shows the extended depth of focus and better contrast (Fig. 1b). Figures 1c and d show a nonconfocal image (pinhole open) and a confocal image (pinhole 100), respectively, of an agglomerate of cells. In the nonconfocal image the individual cells are obscured by stray light, whereas in the confocal image they can be identified more clearly. Video images were photographed on Kodak Ektachrome 100 ASA film with a FreezeFrame Video Recorder (Polaroid Co., Cambridge, Mass.).

The DTAF-stained soil smears were excited at 488 nm with an Omnichrome 155T argon ion laser (2 to 50 mW, 488/514 nm; Omnichrome, Chino, Calif.). A beam splitter of 510 nm and a barrier filter of 530 nm were used. The slides were observed with a 100× 1.32 NA oil immersion objective lens, a laser power of 95,000 (corresponding to 20 mW), a pinhole size of 120 (range, 0 to 255 corresponding to 0 to 100 μm), and a photomultiplier sensitivity of 700 V (range, 0 to 1,000 V).

Image analysis system. CLSM images are transferred to a Quantimet 570 (Q570) image analysis system (Leica Cambridge Ltd., Cambridge, United Kingdom) by means of an RGB (red, green, and blue) video cable which connects the CLSM image monitor with a video input port of the Q570. Thus, the live CLSM image is displayed on the Q570 image display monitor and can be stored in one of 24 grey image planes each of 512 by 512 by 8 bits (6-Mb image memory). The digitized images of 256 grey levels are processed by a programmable logic cell array processor optimized to handle morphological transforms. After image processing, the simplified image is segmented to a binary image (512 by 512 by 1 bit) which is stored in one of 22 binary image planes. The binary image is further processed (simplified) and finally measured by a dedicated feature extraction and measurement processor. Both dedicated processors are controlled and measurements are evaluated by a 68000 microprocessor (512-kb RAM). The whole system is controlled by a 80386 personal computer (20 MHz, 2-Mb RAM, 340-Mb hard disk) which serves as the user interface. Both the CLSM and the Q570 were built in 1990.

The image processing and analysis operations of the Q570 can be operated interactively from the menus of the user interface. Once the appropriate operations have been selected and arranged, they can be inserted in a QBasic application program for automatic operation and data handling. QBasic is a combination of standard Basic commands and specific commands which control the Q570 system. The application program also controls the motorized *x-y* stage containing the specimen in the CLSM and starts the scanning macro of the CLSM at each new field of view. The communication between the Q570 and the CLSM is based on printable ASCII characters transmitted by an RS232 interface. Usually 10 fields of view are scanned. We started with a scan pattern defined by three steps of 1,200 μm in the *x* direction and four steps of 1,000 μm in the *y* direction. It appeared, however, that some microscopic slides were not completely flat in the *y* direction, so that the soil smears ran out of focus when a total thickness of 4.5 μm was scanned. Therefore, we switched to scanning 10 steps of 800 μm in the *x* direction.

Image processing. The Q570 uses mathematical morphology for image processing. The principles have been described by Serra (25, 26). In morphology, a grey image can be imagined as a three-dimensional landscape. The *x* and *y* coordinates represent the extent of the image. The grey level value of each pixel in the image is represented on the vertical or *z* axis. Thus, white points are on top of mountains (snow) while black points are at sea level. Shades of grey represent intermediate values. Morphological operations are performed by a structuring element which moves over the original image, pixel by pixel, to create a new transformed image. On each point, grey values of surrounding points which are covered by the structuring element are used to calculate a new value for the central point. Structuring elements of different shapes can be used to achieve different transformations. The basic grey transformations erosion and dilation can be envisioned as a flat disc moved over the surface. For dilation, it cannot enter the bottoms of the valleys and it extends the sides of the hills. It does not raise the height of the peaks, because the disc is flat. For erosion, the disc is moved under the surface to shrink the sides of the profiles and widen the valleys. Dilation may be described as replacing the grey level of the center point by the maximum grey level found in the structuring element, whereas for erosion the center point is replaced by the minimum grey level.

The basic morphological grey image transforms used for analysis of soil bacteria are demonstrated by using an image in which bacteria are shown at a high magnification (Fig. 2). The image was scanned by the CLSM at a pixel size of 0.049 μm, resulting in Fig. 2e. The cells in the center were magnified by a software zoom operation of the Q570, resulting in an image showing the individual pixels that cover the cells (Fig. 2a). A line was drawn through the central cells in Fig. 2a, and the grey level profile along that line is shown below the image in Fig. 2b. The bacterial cells appear as peaks in the grey level, where 0 represents black and 255 represents the highest light intensity (white). In principle, the bacteria can be measured by setting a threshold for binary segmentation. Segmentation of the original image, however, does not result in an acceptable binary image of the bacteria, because there is a considerable variation in the grey level of the individual pixels, resulting in a noisy image and a rough profile. Therefore,

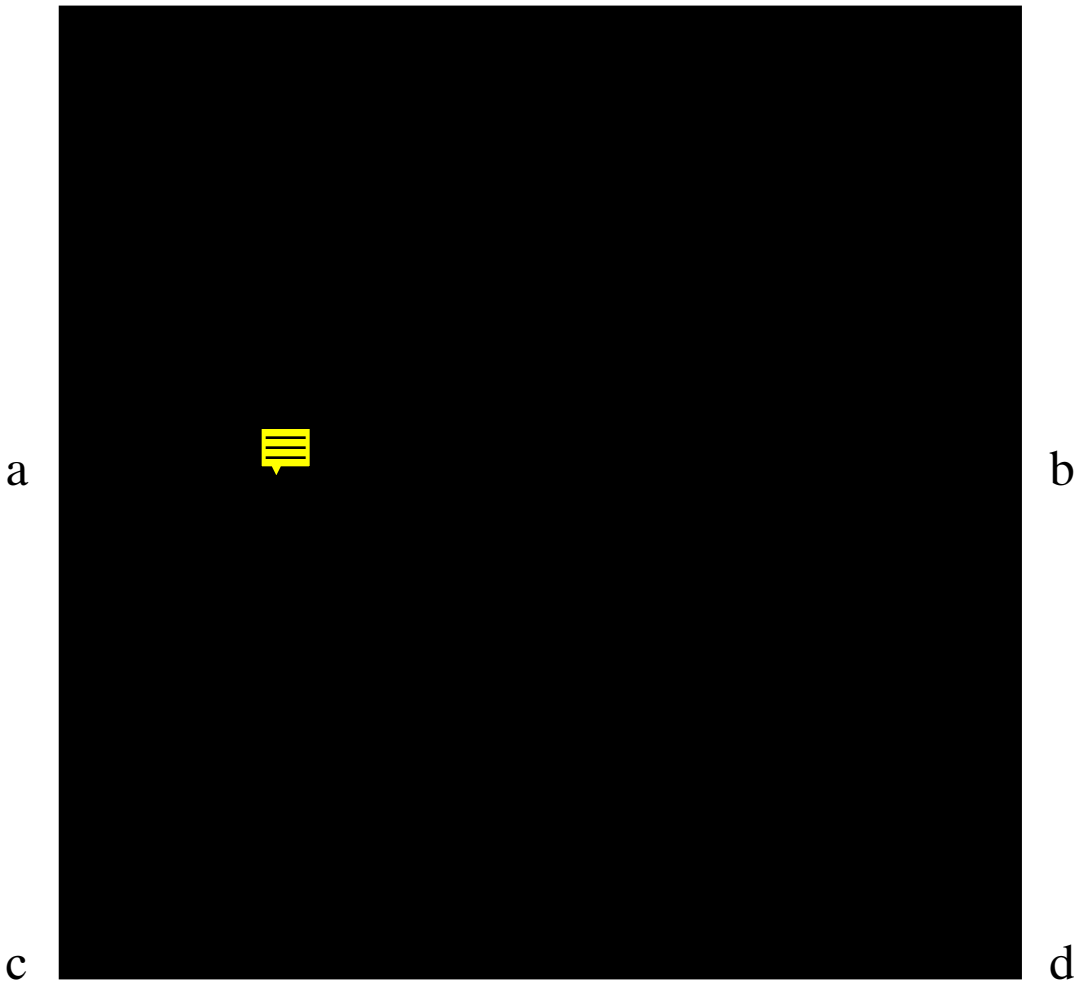

FIG. 1. Comparison of confocal and nonconfocal images. Fluorescently stained bacteria in a soil smear under a conventional epifluorescence microscope (a) and a CLSM (b) and an agglomerate of cells under a CLSM imaged with the pinhole open (nonconfocal) (c) and with the pinhole closed (confocal) (d).

the image is smoothed by averaging the grey value of each pixel with the value of the surrounding pixels, using a 5 by 5 convolution filter:

$$\begin{matrix} 1 & 1 & 1 & 1 & 1 \\ 1 & 1 & 1 & 1 & 1 \\ 1 & 1 & 1 & 1 & 1 \\ 1 & 1 & 1 & 1 & 1 \\ 1 & 1 & 1 & 1 & 1 \end{matrix}$$

Thus, the noise is smeared over a wider area. Next, the profile is further smoothed by morphological opening and closing. Opening is erosion followed by dilation. The erosion removes small peaks and the subsequent dilation restores the original size of the bigger peaks. Thus, peaks are flattened and small white objects are removed. Closing is dilation followed by erosion to fill valleys and to remove small dark objects. The result is a somewhat hazy image and a smooth profile (Fig. 2c). Now a threshold could be set, but the size of the detected cells will decrease when the threshold is increased, because of the slope of the grey level along the cells. Therefore, the hazy image is sharpened by delineation with a morphological minimum/maximum filter. This filter improves the definition of edges by setting the grey level of pixels to the most extreme local minimum or maximum value found in a region defined by the size of the structuring element. Thus, in gradients, intermediate grey levels are removed and only the extreme values are kept. The result is a sharp image with very steep edges in the profile (Fig. 2d). In this image, the threshold used for binary segmentation has little effect on the size of the detected particles. The edges of the detected particles in the binary image are then smoothed by binary closing.

A detected particle may consist of more than one cell. To determine the number of cells in agglomerates, all local maxima in the morphologically smoothed image (Fig. 2c) are detected, resulting in a binary image of detected pixels all over the image. A local maximum is a pixel or a region of pixels completely surrounded by pixels of lower grey level. The degree of smoothing which has been applied previously determines the number of local maxima found. The maxima are dilated one cycle to improve their visibility. Then a logical AND operation is performed on the detected particles and the detected local maxima, resulting in an image of only those local maxima which are located in detected particles. Figures 2e and f show the original image and a binary image displayed as an overlay on the original grey image, respectively. The outlines of the detected particles are marked by a red line, and the local maxima are indicated by a yellow point. Particles containing two local maxima, such as the central cells in Fig. 2c, are counted as dividing cells (labeled D). From these maxima, individual cells are constructed by performing a geodesic skeletonization by influence zone of the maxima, using the detected particles as a mask. An operation is called geodesic when the region of the amendment is constrained to an area defined by another "mask" binary plane. In this case, the skeletonization by influence zone is performed only in detected particles. A skeleton by zone of influence is a combination of exhaustive black (or inverse) skeleton and exhaustive inverse pruning. The black skeleton is formed by thickening the features (local maxima) until they are separated by a single background line one pixel wide. The black skeleton is then pruned to remove dendrites. In the resulting binary image, each feature resides in its own influence zone of set pixels, which is separated from the influence zone of adjacent features by a single-pixel boundary. Thus, an image of separate zones (presumably cells) which contain the pixels nearest to each maximum is produced.

These principles were used for the first version of our image analysis program for bacteria. This version, however, was semiautomatic because thresholds were set manually and complex images with high background staining had to be edited interactively. Also, the number of cells per agglomerate could be edited. In April 1991, a new version of the Q570 software (QUIC version 2.00) included three-dimensional structuring elements such as a rhombododecahedron, which is an approximation of a sphere. We found that this spherical structuring element could be used for fully automatic background correction. Figure 3a shows a very

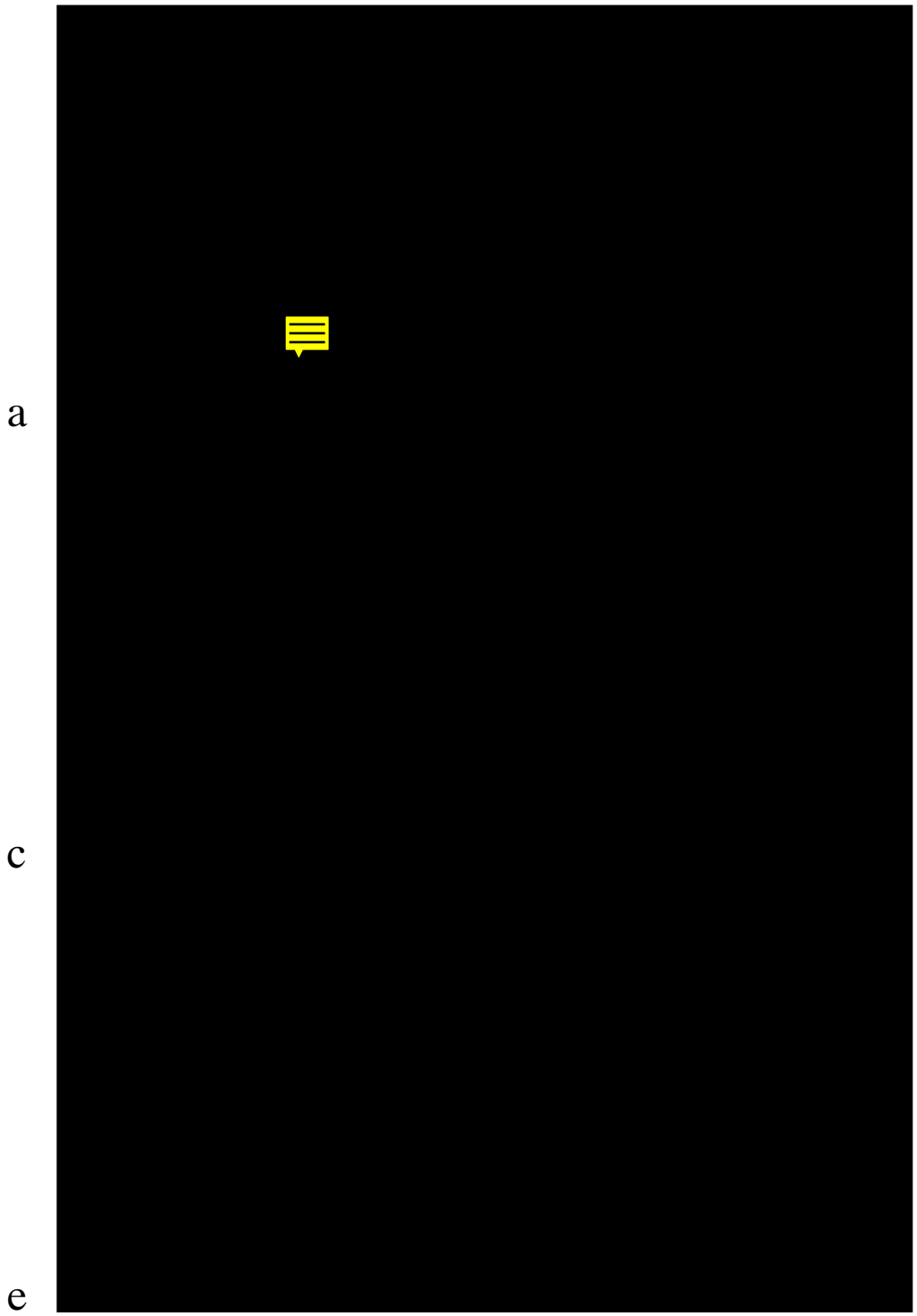

FIG. 2. Basic morphological grey image transforms shown at high magnification. (a) Detail of an original image with a green line through the bacteria in the center; (b) grey level profile along the line in panel a (y axis = grey level; x axis = distance in pixels); (c) image and profile after smoothing by opening and closing, showing two local maxima; (d) image and profile after sharpening by delineation; (e) whole original image of 512 by 512 pixels (pixel size, 0.049 μm); (f) final image after binary segmentation of the sharpened image at grey level 80. Red line, cell outline; yellow spot, local maximum indicating the center of a cell; S, single cell; D, dividing cell; A, agglomerate of more than two cells.

complex image (pixel size, 0.098 μm) with a high and irregular background staining which complicates the detection of bacteria. Moreover, in the lower left corner there is a brightly stained big particle which is clearly not a bacterium. Although such bad images are rare, we used this image to develop a fully automatic application program which can handle virtually all our images satisfactorily. The grey level profile along the green line in Fig. 3a is shown in Fig. 4a. The image is first smoothed as described above, resulting in Fig. 3b and 4b. To facilitate later subtraction of the background, the background is then equalized by flooding holes (depressions) in the image to a consistent grey level (Fig. 3c and 4c). The equalized background is subtracted by two subsequent morphological

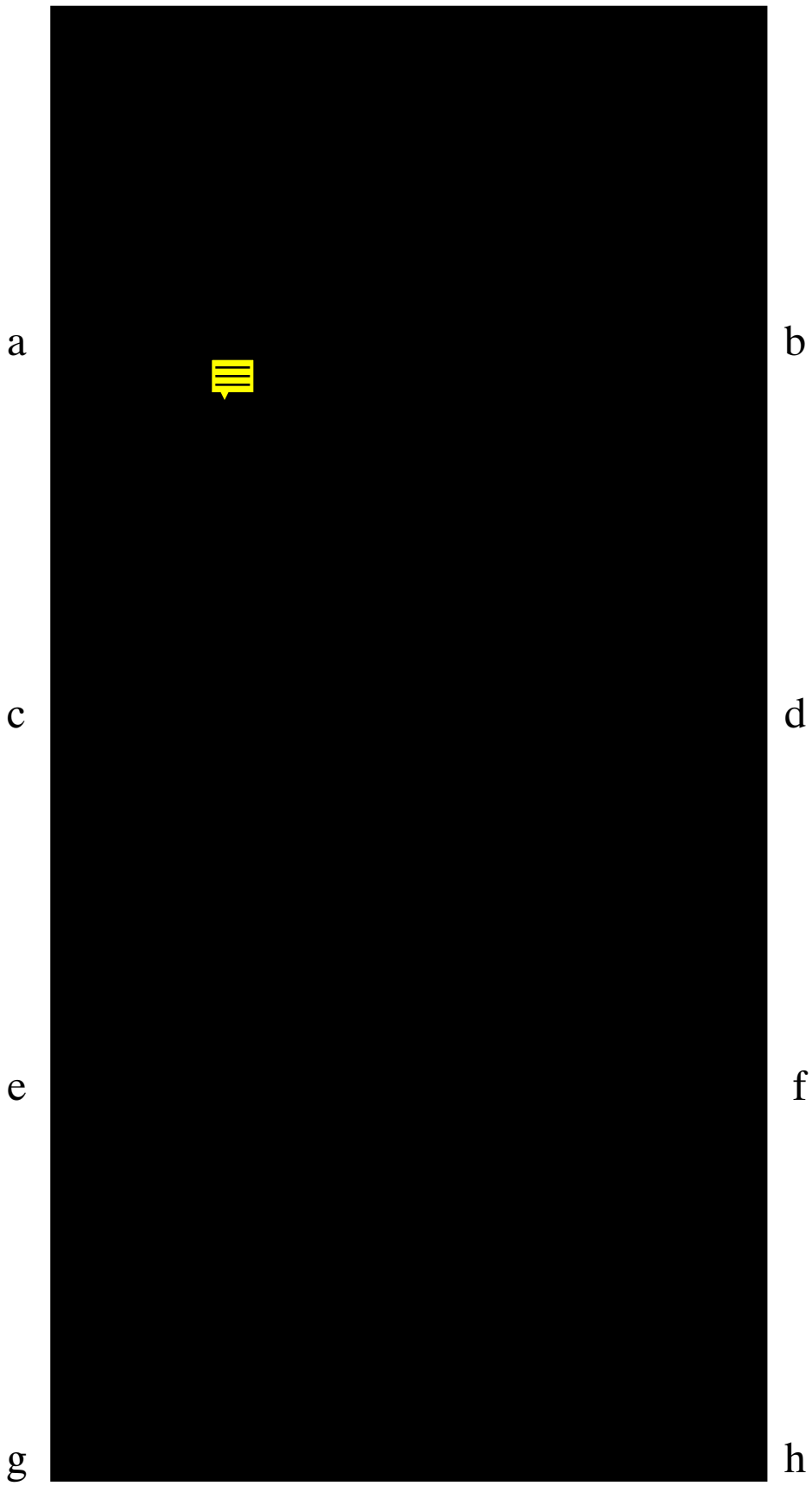

FIG. 3. Fully automatic processing of a complex image of soil bacteria. (a) Original grey image (pixel size, 0.098 μm) from the CLSM; (b) noise reduced by smoothing; (c) holes in background and particles filled by flooding; (d) background subtracted by a top hat transform with a disc-shaped structuring element; (e) background further eliminated by a top hat transform with a spherical structuring element; (f) image sharpened by delineation; (g) binary image after application of a threshold at a fixed grey level of 25; (h) individual cells reconstructed from local maxima.

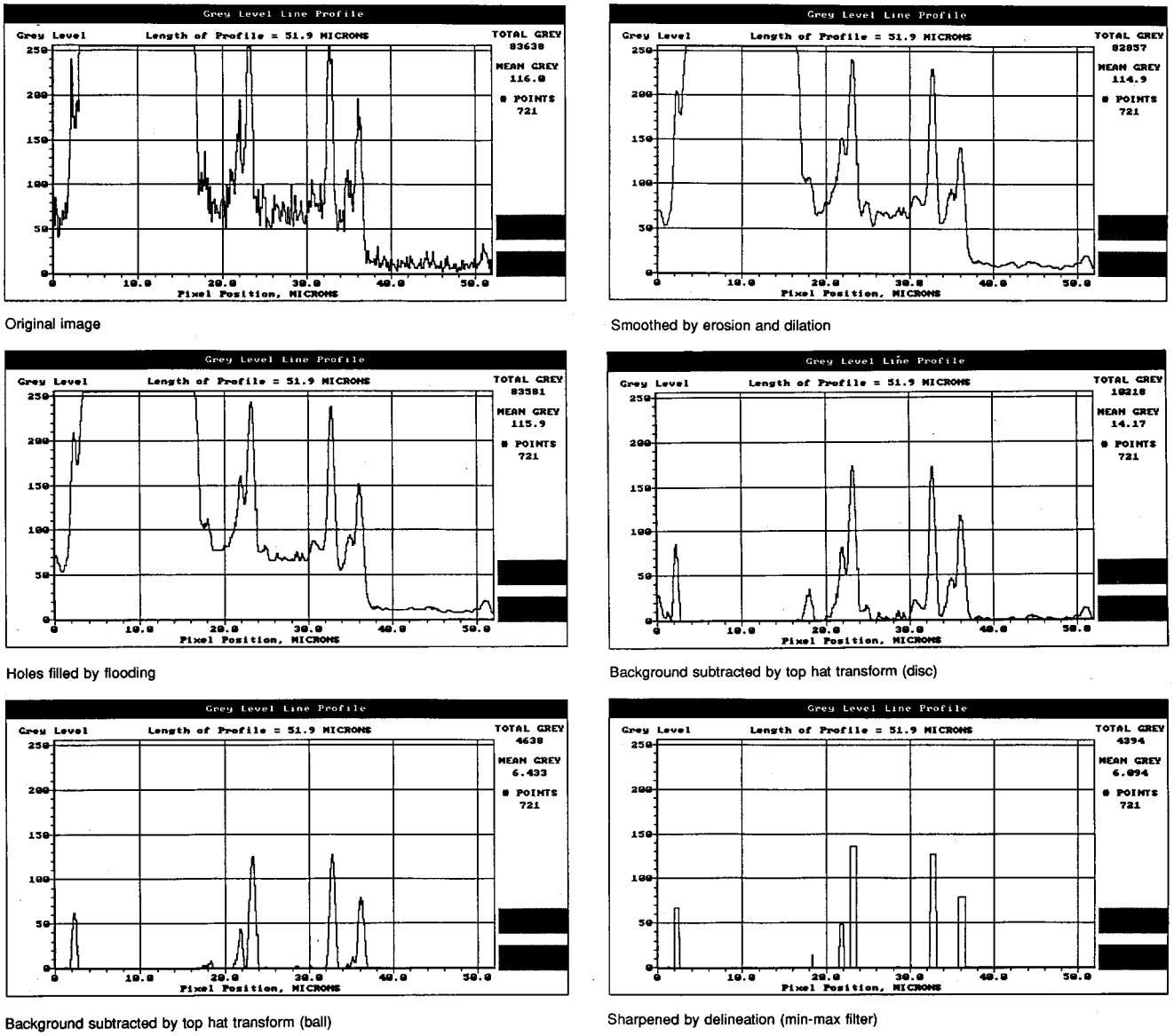

FIG. 4. Principles of image processing demonstrated with the grey level profile along an approximately 50-μm line in a complex image (green line in Fig. 3). Panels a to f correspond to Fig. 3a to f, respectively.

top hat transforms (Quantimet 570 Operators Manual, no. GL-428472; Leica Cambridge Ltd.) based on the method of Serra (25). A top hat transform is performed by first removing small peaks by opening. The remaining bigger peaks (background) are subtracted from the original image, and then only smaller peaks (white detail) remain. The size of the detail retained depends on the size of the opening (which was set at 20; range, 1 to 512). The first top hat transform is performed with a disc-shaped structuring element (size 20) that removes most of the background (Fig. 3d and 4d). The remaining background is reduced further by the second top hat transform with a spherical structuring element (size 20; *z* or grey level dimension, 5) (Fig. 3e and 4e). If small holes in the background are not filled before the background subtraction, they can cause artificial small particles remaining after the top hat transforms. After background subtraction, the image is sharpened by delineation (Fig. 3f and 4f) and segmented into a binary image by using a fixed threshold with a grey value of 25 (Fig. 3g). Finally, the individual cells are reconstructed from local maxima by using geodesic skeletonization by zone of influence (Fig. 3h). If a detected particle contains no local maximum, such as some particles on the edge of the big particle in Fig. 3, it is not reconstructed to a cell in the final image (cf. Fig. 3g and h). The total image-processing procedure is summarized in Fig. 5.

Image analysis. The number of cells in each detected particle is determined by counting the number of coincident particles in bitplane (binary image plane) 4 (local maxima) and bitplane 1 (detected cells and agglomerates of cells) (Fig. 5). Agglomerates of two cells are assumed to be dividing cells. All individual cells (bitplane 7) are counted, and the length and width of each cell are determined by measuring the fiber length and fiber width, which are defined as follows:

$$\text{Fiber length} = [\text{perimeter} + \sqrt{(\text{perimeter}^2 - 16\ \text{area})}]/4$$

$$\text{Fiber width} = [\text{perimeter} - \sqrt{(\text{perimeter}^2 - 16\ \text{area})}]/4$$

These parameters can be described as the length (longest side) and width (shortest side) of a rectangle having the same area and perimeter as the measured particle. If (perimeter^2 − 16 area) is negative, which is the case for spheres, the Q570 takes the equivalent circle diameter as length and width. This parameter is defined as the diameter of a circle having the same area as the measured particle. Estimates of length and width based on area and perimeter are more stable and reliable than estimates based on the maximum and minimum diameters (3, 17). Cell volumes are calculated as follows (20):

$$\text{Volume} = (\pi/4)\ \text{width}^2\ (\text{length} - \text{width}/3)$$

During the analysis, the results for successive fields of view are accumulated in five histograms showing the frequency distributions of cell volume (64 size classes between 0 and 2 μm^3), length (0 to 6.4 μm, 64 classes), width (0 to 6.4 μm, 64

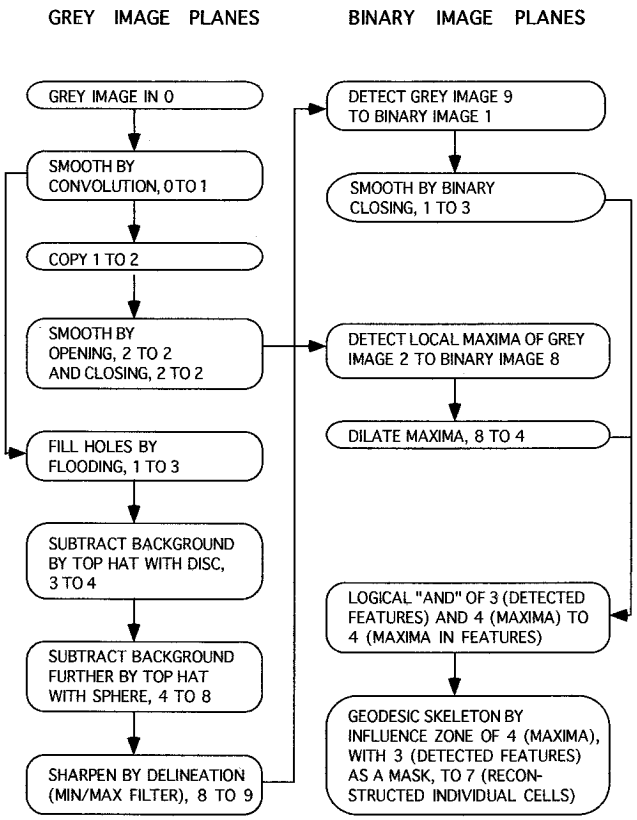

FIG. 5. Flow chart of the image-processing program. The numbers refer to the numbers of the grey image planes and of the binary image planes used in the Quantimet; e.g., an image stored in plane 0 is transformed, and the resulting image is stored in plane 1.

classes), length-to-width ratio (1 to 17, 16 classes), and number of cells per agglomerate (1 to 17, 16 classes). The mean, median, and standard deviation of each parameter, as well as the number of cells and the number of fields measured, are also tabulated. After analysis, statistics and histograms are automatically printed and saved to disk. Also, the results for all individual cells in all separate fields are automatically saved to disk. As an option, the images of all successive fields can be saved automatically for visual inspection afterwards.

Control measurements. The results of image analysis of soil bacteria were demonstrated by measurements in substrate-amended microcosms. Silt loam soil was spread out and dried for 2 days at 2°C. A series of pots were filled with 20 g of dry soil, which was mixed with 200 mg of tryptone soy broth (Oxoid Ltd., Basingstoke, United Kingdom) in 5 ml of water. The pots were incubated at 10°C for eight periods between 0 and 21 days. On each sampling day, bacteria were measured in samples from three microcosms. Only results from days 0 and 2 are reported.

Automatic counts of bacterial numbers and FDC performed by image analysis were compared with visual counts (9) on the same slides, prepared from three replicate samples taken from the Lovinkhoeve experimental farm on each of three sampling dates in 1991.

Cell volume measurements were evaluated by measuring yellow-green fluorescent polystyrene latex microspheres of known size (no. L-5261, L-5281, and L 5301, calibration grade, 51 μmol of dye g of polystyrene^{-1}; Molecular Probes Inc., Eugene, Oreg.). In addition, cell volume measurements were evaluated by simultaneous determination of cell carbon, cell numbers, and cell volumes in samples of bacteria grown in continuous culture. A mixture of *Alcaligenes* sp., *Arthrobacter* sp., and *Corynebacterium michiganense*, all isolated from soil (22), was grown on tryptone soy broth (0.3 g liter^{-1}) at 15°C at four different generation times (21). DTAF-stained bacteria were measured by image analysis, and bacterial carbon was determined in acidified samples on a model 500 total organic carbon analyzer (Shimadzu Co., Kyoto, Japan). Total carbon in the sample was combusted at 680°C, oxidized to CO_2, and measured with a nondispersive infrared detector. Cell carbon was assumed to be the difference between the C content of unfiltered and 0.2-μm-pore-size-filtered (polycarbonate membrane) culture fluid (21).

RESULTS

Microcosms. After rewetting and amendment, bacterial numbers in the microcosms increased strongly from 0.65×10^9 cells g of soil^{-1} on day 0 to 6.04×10^9 cells g of soil^{-1} on day 2. Analysis of variance yielded a significance of $P < 0.0001$ and a least significant difference (LSD) of 1.46×10^9. The high bacterial growth rate resulted in shifts in the frequency distributions of cell length, width, volume, and number of cells per

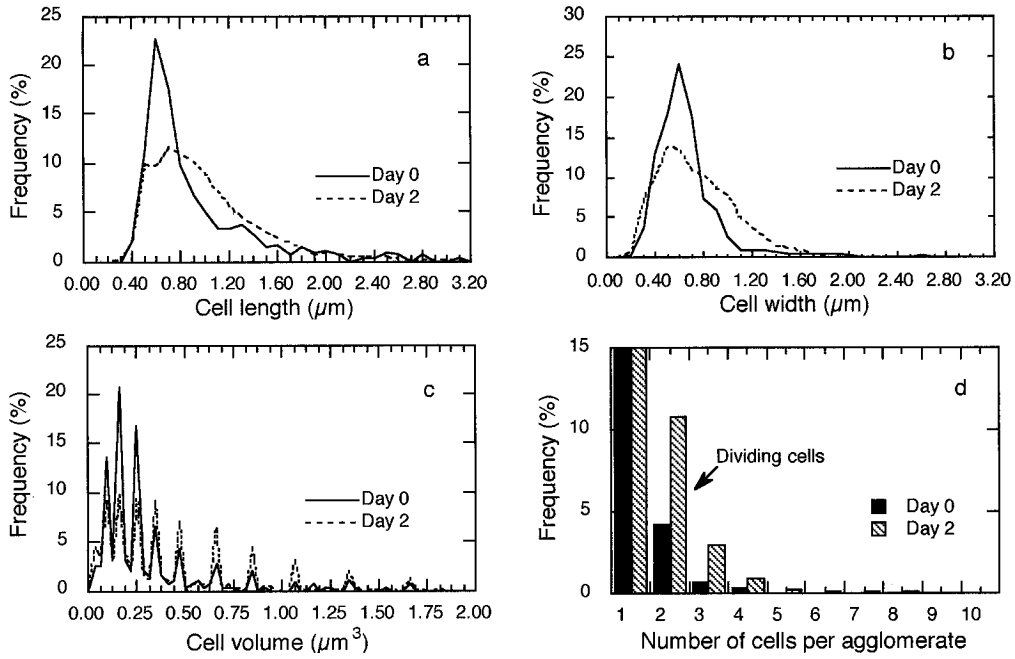

FIG. 6. Results of automatic image analysis. Frequency distributions of length, width, volume, and number of cells per agglomerate of bacteria in microcosms 0 and 2 days after amendment with tryptone soy broth.

TABLE 1. Comparison of visual and automatic counts of bacterial numbers and FDC in field samples[a]

Date (1991)	No. of bacteria (10^9 bacteria g of soil^{-1})					FDC (%)				
	Visual		Automatic		Vis/auto ratio	Visual		Automatic		Vis/auto ratio
	Mean	CV (%)	Mean	CV (%)		Mean	CV (%)	Mean	CV (%)	
28 Feb	2.45	9	1.93	48	1.27	4.42	2	4.54	23	0.97
9 Apr	3.15	15	3.24	24	0.97	3.80	13	4.40	27	0.86
13 Aug	1.20	16	0.79	31	1.52	3.42	27	4.95	26	0.69
Mean		13		34	1.25		14		25	0.84

[a] Three soil smears from each sampling date were counted by both methods.

agglomerate (Fig. 6). The average total number of cells measured in 10 fields was 117 on day 0 and 1,101 on day 2. The mean cell length increased from 1.02 to 1.13 μm ($P < 0.0001$; LSD = 0.05 μm), the mean width increased from 0.76 to 0.84 μm ($P < 0.0001$; LSD = 0.03 μm), and the mean volume increased from 0.32 to 0.45 μm^3 ($P < 0.0001$; LSD = 0.03 μm^3). The regular pattern of peaks in the histogram of the cell volume is caused by the digitization of the image in pixels. Length and width do not increase continuously but in discrete steps. The smallest increase of one pixel (0.098 μm) in length causes an increase of 0.03 μm^3 in volume, which is the difference between two successive size classes in the histogram. The peaks occur because the width is squared in the calculation of the volume. The mean length-to-width ratio (data not shown) increased from 1.41 on day 0 to 1.53 on day 1 and decreased again to 1.45 on day 2 ($P = 0.0003$; LSD = 0.06). The frequency of single cells decreased from 95 to 84.8%, while agglomerates of two cells increased from 4.1 to 10.8% of the total number of agglomerates. The FDC, calculated as the number of agglomerates with two cells divided by the total number of cells, multiplied by 100, increased from 4.1 to 9.6% ($P = 0.0012$; LSD = 2.0%). Also, the frequency of agglomerates of more than two cells increased (Fig. 6d). The biggest agglomerates found consisted of eight cells and were detected at a frequency of 0.1%. Cells in agglomerates of more than two cells were assumed to be nondividing and were included in the total number of cells used for calculation of the FDC.

Visual and automatic counts. Visual and automatic counts of bacterial numbers and FDC in nine soil smears of field samples yielded similar results (Table 1). The mean differences between the methods were not significantly different from zero (Student's *t* test). Both methods showed a significant effect of sampling date on bacterial numbers ($P = 0.016$) but not on the FDC (analysis of variance). Although for these nine slides the differences in variance between the methods were not significant (F test), our experience is that the coefficient of variation in automatic counts is about twice as high as in visual counts.

Specified and measured volumes of microspheres. Because the fluorescent microspheres were much brighter than bacteria, they had to be measured at a lower photomultiplier sensitivity. A major problem is that bigger spheres are much brighter than smaller spheres because staining intensity is proportional to volume. When the sensitivity was optimized for each size class separately, a difference of less than 10% between the specified and measured volumes was obtained, except for the smallest beads (diameter, 0.42 μm), which were always overestimated by one pixel. In normal samples, cells of different size and brightness have to be analyzed simultaneously in the same image, and so only one setting of the sensitivity can be used. Therefore, the three size classes of beads were all measured at the same photomultiplier sensitivity of 515 V. The 0.98-μm-diameter beads, which have a volume close to that of bacteria (Fig. 6), were measured accurately (Table 2). The 0.42-μm-diameter beads represented the smallest bacterial size class measured (Fig. 6), and the 70% overestimation of the volume represented only one pixel. The diameter of the 2.47-μm-diameter beads was overestimated by 8% (two pixels), which resulted in a 25% overestimation of the calculated volume. The biggest microspheres, however, were much bigger than soil bacteria (Fig. 6). The measured size could be decreased by decreasing the photomultiplier sensitivity, but then the grey value of the smallest beads (after image processing) decreased to below the threshold grey value of 25 used for detection of bacteria in field samples. Although the absolute values of the volumes were overestimated, the ratios between the volumes of the three size classes were measured with good approximation. The nominal volumes were related as 0.08:1.0:16, and the measured volumes were related as 0.12:1.0:19. This illustrates that the relative values are correct but the absolute numbers and volumes obtained are very sensitive to the settings of photomultiplier sensitivity and the threshold used for binary segmentation. These settings are still rather subjective choices of the operator. We minimized this problem by choosing (subjectively) settings which yielded satisfactory results with images of field samples (such as in Fig. 4) and by keeping all settings constant in later measurements.

Cell volumes and directly measured cell carbon. It is difficult to translate results with microspheres to results with bacteria, because with bacteria the relationship between size and brightness seems to be less consistent. Therefore, measurements of biovolumes (cubic micrometer per cell) were compared with independent direct cell carbon measurements (femtograms of

TABLE 2. Comparison of specified and measured mean diameters and volumes of fluorescent latex microspheres[a]

Specified diam (μm)		Measured diam (μm)		Overestimation of diam (%)	Specified vol (μm^3)	Measured vol (μm^3)		Overestimation of vol (%)
Mean	CV (%)	Mean	CV (%)			Mean	CV (%)	
0.42	7.9	0.49	9.6	17	0.037	0.063	31	70
0.98	2.6	0.99	5.9	1	0.49	0.52	18	6
2.47	4.6	2.67	20.8	8	7.9	9.9	28	25

[a] n = 197, 179, and 113 for the 0.42-, 0.98-, and 2.47-μm-diameter beads, respectively. Pixel size, 0.098 μm.

TABLE 3. Comparison of bacterial cell volumes determined by image analysis and directly measured bacterial carbon in samples from mixed continuous cultures of *Alcaligenes* sp., *Arthrobacter* sp., and *Corynebacterium michiganense* grown at four generation times[a]

Generation time (days)	Bacterial carbon ($\mu g\ ml^{-1}$)	No. of cells ($10^8\ ml^{-1}$)	Cell vol ($\mu m^3\ cell^{-1}$)	Cell carbon content ($fg\ cell^{-1}$)	Specific carbon content ($fg\ \mu m^{-3}$)
1.2	33.4 ± 4.9	5.7 ± 0.5	0.41 ± 0.05	59 ± 4	146 ± 26
1.7	39.1 ± 0.2	5.6 ± 0.6	0.25 ± 0.07	71 ± 7	287 ± 44
3.5	20.5 ± 3.0	3.9 ± 0.3	0.39 ± 0.07	53 ± 12	139 ± 28
4.1	24.9 ± 1.3	4.7 ± 0.5	0.25 ± 0.03	53 ± 7	212 ± 39

[a] Values are expressed as means and standard deviations of three determinations.

carbon per cell) in samples from continuous cultures (Table 3). From these data, an average specific carbon content of 196 ± 69 fg of C μm^{-3} (mean ± standard deviation; $n = 12$) was calculated. At different generation times, we found significantly different cell volumes ($P = 0.012$; LSD = 0.10 μm^3). Consequently, the specific carbon content also differed significantly between generation times ($P = 0.003$; LSD = 66 fg of C μm^{-3}). There was no simple relationship between growth rate and cell volume. This may have been caused by different relative abundances of the three species at the different growth rates. In contrast to the cell volume, the cell carbon content was not significantly different at different generation times.

DISCUSSION

The integrated combination of the CLSM and the Q570 is, to our knowledge, the first system that provides fully automatic image analysis of bacteria, the first that handles bacteria in soil samples, and the first that identifies and counts dividing cells. The system is commercially available from Leica, and the application program described here is available from the authors. Ten fields of view in one slide, which may contain up to 1,500 cells in total, are scanned and analyzed in 30 min. Between focusing the first field and printing the results, no operator is required. Systems described previously were semiautomatic, since image acquisition, interactive editing of unwanted background, and sometimes binary segmentation (application of a threshold) were performed manually (3, 29). The key to fully automatic image analysis with our system was the automatic background correction by the top hat transforms with the two-dimensional disc-shaped and the three-dimensional spherical structuring elements (Fig. 3 and 4). Without these transforms, thresholds had to be set manually in each image and in some images background had to be removed by manual editing. After automatic background subtraction, one fixed threshold could be used for all images.

Automatic counts of soil bacteria have the same limitation as visual counts in soil smears: bacteria may be masked by soil particles. To avoid severe masking, the soil is diluted at least 10-fold with water, so that less than 1 mg of soil is smeared on 1 cm^2 of the microscopic slide (5). Moreover, coarse particles are removed by settling for 2 min before the smears are prepared. Babiuk and Paul (2) added known amounts of bacteria to soils with clay contents ranging from 20 to 80% and recovered 95 to 101% of the added bacteria in soil smears. However, even in sufficiently diluted soil, some masking will occur. Methods have been proposed to estimate the number of hidden bacteria (17), but we find them complicated and did not attempt to correct the numbers counted for masking by particles.

Automatic counts of dividing cells are facilitated by the good contrast and high resolution of the CLSM and by the detection of local maxima by the Q570. By using a 100× 1.32 NA objective at an excitation wavelength of 488 nm, an *x/y* resolution of 0.2 μm and a *z* resolution of 0.4 μm can be achieved with the CLSM, which is 1.4 times higher than with a nonconfocal microscope (15). Dividing cells have been defined by Hagström et al. (18) as "bacteria showing an invagination, but not a clear intervening zone between cells." In our image analysis program, dividing cells are defined as pairs (agglomerates) of two adjacent cells which are identified by two local grey level maxima within one detected particle (Fig. 2c). We think that both definitions have the same result: pairs of adjacent cells are identified and assumed to be dividing. Since agglomerates of more than two cells have never been included in the definition of dividing cells (18), and since we prefer conservative estimates, such agglomerates are arbitrarily assumed to be nondividing. The growth experiment with the microcosms showed that the FDC can be a useful indicator of increased specific growth rates of soil bacteria (Fig. 6). Since the FDC method is not very sensitive at low growth rates, since dividing cells may be preferentially grazed by protozoa (28), and since nongrowing diplococci may be present, it is better to combine the FDC method with other methods for estimating the growth rate of soil bacteria, such as tritiated thymidine incorporation (1, 21). The thymidine method is more sensitive but has the disadvantage that not all bacteria are able to incorporate thymidine. The FDC method yielded useful results in studies on the dynamics of bacteria and nitrogen mineralization in arable fields (6, 7) and becomes much more attractive when the FDC can be determined automatically.

Automatic image analysis of soil bacteria yields more objective and quantitative results than do visual estimates. Size estimates based on the number of pixels covering a cell are much more accurate than visual estimates obtained with an ocular micrometer. In our soil samples, an average cell (length, 1.0 μm; width, 0.6 μm) is covered by about 40 pixels with a size of 0.10 by 0.10 μm. For comparison, the smallest division on our ocular micrometer is 0.47 μm. The image analysis system always uses the same thresholds and criteria to detect and measure cells. When a complex image is analyzed twice, the results are identical. Nevertheless, the coefficient of variation (CV) of automatic counts of bacterial numbers (about 30%) appeared to be about three times higher than the CV of visual counts (about 10%) (Table 1). The variance-to-mean ratio of the mean number of bacteria per field was significantly ($P = 0.0001$) higher in the automatic counts (10.5 ± 6.0) than in the visual counts (2.4 ± 0.8) (means ± standard deviations; $n = 9$). This suggests a more contagious (patchy) distribution of bacteria (9) on the slides in the automatic counts, i.e., a greater variation in numbers between fields. In the visual counts, the numbers appeared to be more randomly spread over the fields. Since the slides used for the automatic counts were the same as those used for the visual counts, the difference in the distribution of bacteria on the slides must have been apparent. Probably, a human observer expects a certain number of cells per field and tends to underestimate numbers in fields with many cells and may overestimate numbers in fields containing few

cells. This may result in an (apparently) lower CV. We could not reduce the variation by more vigorous homogenization of soil suspensions or by addition of sodium PP_i and detergents (Tween 80 and sodium hexametaphosphate) (5). Blending for up to eight 1-min pulses (instead of the usual 1 min) at maximum speed (23,000 rpm) in a Waring blender, mixing for 10 min at 15,000 rpm in a Silverson mixer emulsifier, and sonication for up to 5 min with an MSE Soniprep 150 (maximum power) did not reduce the CV, although the last two treatments reduced the numbers by 40 to 80%. Also, the use of membrane filters instead of soil smears for automatic counts did not reduce the average variation among soil samples below 30%. With water samples on membrane filters, we obtained a somewhat lower CV of 20% ($n = 10$), which is similar to the variation found with the image analysis system described by Viles and Sieracki (28a, 31).

Although volumes of fluorescent microspheres of different sizes were measured relatively well (Table 2), the absolute values depended on the sensitivity settings of the detector. For the calibration, we used microspheres of different sizes with the same specific dye content (51 μmol of dye g of polystyrene^{-1}). If particles with different dye contents and hence different brightness were used, different sensitivity settings were needed for correct volume measurement. Since bacteria may differ greatly in specific dye content and brightness, volumes of dim cells may be underestimated and volumes of bright cells may be overestimated. The problem of accurate sizing of fluorescent particles with different brightnesses has been investigated thoroughly by Sieracki et al. (30), and algorithms for automatic edge detection of bacteria in water samples have been published. These methods are based on detection of local changes in brightness (gradients) by using first or second derivatives and are less dependent on the absolute grey levels (and background) in the image. Schröder and Krambeck (24) used the maximum of the first derivative, which produced a white ring at the cell edge. Viles and Sieracki (31) used the zero crossings of the second derivative (Marr-Hildreth method) combined with an edge strength operator which evaluates the strength of the edge before it is detected. We have tried edge detection by both first and second derivatives but were not able to obtain acceptable results with soil samples. For water samples, the gradient methods were applied directly to the original image without any background subtraction. In fact, the gradient methods were used to detect cells within a fuzzy and cloudy background (24) We obtained poor results with the gradient methods in soil samples without automatic background correction. The results were better after background correction with the top hat transforms, but considerably fewer cells were detected than by our standard delineation followed by application of a threshold.

Our estimates of cell volumes are based on fiber length and fiber width, which are calculated from the measured area and perimeter. With fluorescent microspheres, these estimates were more stable and reliable than volume estimates based on maximum and minimum diameters (length and width). Bjørnsen (3) also estimated cell volumes from area and (convex) perimeter by using the following empirical formula: volume = 8.5 area$^{2.5}$/convex perimeter^2. When we applied this formula on the Q570 to determine volumes of fluorescent microspheres 0.42 μm in diameter, we found a 25% underestimation of the volume, which was caused by a 7.2% overestimation of the convex perimeter. For the bigger microspheres, the underestimation of the volume was about 15%. Since in the same images fiber length and fiber width were measured correctly and yielded the correct volume, we prefer this method. The comparison of measured cell volumes (cubic micrometers per cell) and independently measured cell carbon (femtograms of carbon per cell) (Table 3) yielded an average specific carbon content of 200 fg μm^{-3}. This value is lower than the mean value of 350 fg μm^{-3} found by Bjørnsen (3) but similar to values reported by others (8, 12, 23), which indicates that our volume estimates are reasonable.

Automatic image analysis is a great improvement over visual counts, because much more quantitative measurements can be performed much more objectively in a shorter time. Cell number, FDC, and detailed frequency distributions of cell volume, length-to-width ratio, and the number of cells per agglomerate in a soil smear can be determined fully automatically in 30 min. Although the measurements are of high relative value, it must be realized that the absolute value is still limited. It is still a problem to measure volumes of particles with different brightnesses correctly, and the operator still has to decide what is regarded as a bacterium and what is regarded as background. The advantage of automatic image analysis is that the criteria can at least be defined and standardized.

ACKNOWLEDGMENTS

We thank P. R. Bolhuis and J. Wieringa for technical assistance, P. H. Michel for providing the samples and carbon data of the continuous cultures, J. B. T. M. Roerdink for useful advice on top hat transforms, and M. E. Sieracki and P. C. de Ruiter for comments on the manuscript.

REFERENCES

1. **Bååth, E.** 1990. Thymidine incorporation into soil bacteria. Soil Biol. Biochem. **22:**803–810.
2. **Babiuk, L. A., and E. A. Paul.** 1970. The use of fluorescein isothiocyanate in the determination of the bacterial biomass of grassland soil. Can. J. Microbiol. **16:**57–62.
3. **Bjørnsen, P. K.** 1986. Automatic determination of bacterioplankton biomass by image analysis. Appl. Environ. Microbiol. **51:**1199–1204.
4. **Blakeslee, D., and M. G. Baines.** 1976. Immunofluorescence using dichlorotriazinylaminofluorescein (DTAF). I. Preparation and fractionation of labelled IgG. J. Immunol. Methods **13:**305–320.
5. **Bloem, J., P. R. Bolhuis, M. R. Veninga, and J. Wieringa.** Microscopic methods for counting bacteria and fungi in soil. *In* K. Alef and P. Nannipieri (ed.), Methods in applied soil microbiology and biochemistry, in press. Academic Press, Ltd., London.
6. **Bloem, J., P. C. de Ruiter, G. J. Koopman, G. Lebbink, and L. Brussaard.** 1992. Microbial numbers and activity in dried and rewetted arable soil under integrated and conventional management. Soil Biol. Biochem. **24:**655–665.
7. **Bloem, J., G. Lebbink, K. B. Zwart, L. A. Bouwman, S. L. G. E. Burgers, J. A. de Vos, and P. C. de Ruiter.** 1994. Dynamics of microorganisms, microbivores and nitrogen mineralisation in winter wheat fields under conventional and integrated management. Agric. Ecosyst. Environ. **51:**129–143.
8. **Bloem, J., M. Starink, M.-J. B. Bär-Gilissen, and T. E. Cappenberg.** 1988. Protozoan grazing, bacterial activity, and mineralization in two-stage continuous cultures. Appl. Environ. Microbiol. **54:**3113–3121.
9. **Bloem, J., D. K. van Mullem, and P. R. Bolhuis.** 1992. Microscopic counting and calculation of species abundances and statistics in real time with an MS-DOS personal computer, applied to bacteria in soil smears. J. Microbiol. Methods **16:**203–213.
10. **Brakenhoff, G. J., H. T. M. van der Voort, J. L. Oud, and A. Mans.** 1990. Potentialities and limitations of confocal microscopy for the study of 3-dimensional biological structures, p. 19–28. *In* B. Herman and K. Jacobson (ed.), Optical microscopy for biology. Wiley-Liss, New York.
11. **Brakenhoff, G. J., H. T. M. van der Voort, E. A. van Spronsen, W. A. M. Linnemans, and N. Nanninga.** 1985. Three-dimensional chromatin distribution in neuroblastoma nuclei shown by confocal scanning laser microscopy. Nature (London) **317:**748–749.
12. **Bratbak, G., and I. Dundas.** 1984. Bacterial dry matter content and biomass estimations. Appl. Environ. Microbiol. **48:**755–757.
13. **De Ruiter, P. C., J. Bloem, L. A. Bouwman, W. A. M. Didden, G. H. J. Hoenderboom, G. Lebbink, J. C. Y. Marinissen, J. A. de Vos, M. J. Vreeken-Buijs, K. B. Zwart, and L. Brussaard.** 1994. Simulation of dynamics in nitrogen mineralisation in the belowground food webs of two arable farming systems. Agric. Ecosyst. Environ. **51:**199–208.
14. **De Ruiter, P. C., J. C. Moore, K. B. Zwart, L. A. Bouwman, J. Hassink, J. Bloem, J. A. de Vos, J. C. Y. Marinissen, W. A. M. Didden, G. Lebbink, and L. Brussaard.** 1993. Simulation of nitrogen mineralisation in belowground food webs of two winter wheat fields. J. Appl. Ecol. **30:**95–106.

15. **Engelhardt, J., and W. Knebel.** 1993. Leica TCS—the confocal laser scanning microscope of the latest generation: technique and applications. Sci. Tech. Inf. **10:**159–168.
16. **Estep, K. W., F. MacIntyre, E. Hjörleifsson, and J. M. Sieburth.** 1986. MacImage: a user-friendly image-analysis system for the accurate mensuration of marine organisms. Mar. Ecol. Prog. Ser. **33:**243–253.
17. **Fry, J. C.** 1990. Direct methods and biomass estimation. Methods Microbiol. **22:**41–85.
18. **Hagström, Å., U. Larsson, P. Hörstedt, and S. Normark.** 1979. Frequency of dividing cells, a new approach to the determination of bacterial growth rates in aquatic environments. Appl. Environ. Microbiol. **37:**805–812.
19. **Hassink, J., L. A. Bouwman, K. B. Zwart, J. Bloem, and L. Brussaard.** 1993. Relationships between soil texture, physical protection of organic matter, soil biota, and C and N mineralization in grassland soils. Geoderma **57:**105–128.
20. **Krambeck, C., H.-J. Krambeck, and J. Overbeck.** 1981. Microcomputer assisted biomass determination of plankton bacteria on scanning electron micrographs. Appl. Environ. Microbiol. **42:**142–149.
21. **Michel, P. H., and J. Bloem.** 1993. Conversion factors for estimation of cell production rates of soil bacteria from [^{3}H]thymidine and [^{3}H]leucine incorporation. Soil Biol. Biochem. **25:**943–950.
22. **Nijhuis, E. H., M. J. Maat, I. W. E. Zeegers, C. Waalwijk, and J. A. van Veen.** 1993. Selection of bacteria suitable for introduction into the rhizosphere of grass. Soil Biol. Biochem. **25:**885–895.
23. **Scavia, D., and G. A. Laird.** 1987. Bacterioplankton in Lake Michigan: dynamics, controls, and significance to carbon flux. Limnol. Oceanogr. **32:** 1017–1033.
24. **Schröder, D., and H.-J. Krambeck.** 1991. Advances in digital image analysis of bacterioplankton with epifluorescence microscopy. Verh. Int. Ver. Limnol. **24:**2601–2604.
25. **Serra, J.** 1982. Image analysis and mathematical morphology. Academic Press, Ltd., London.
26. **Serra, J.** 1986. Introduction to mathematical morphology. Comput. Vision Graphics Image Process. **35:**283–305.
27. **Sherr, B. F., E. B. Sherr, and R. D. Fallon.** 1987. Use of monodispersed, fluorescently labeled bacteria to estimate in situ protozoan bacterivory. Appl. Environ. Microbiol. **53:**958–965.
28. **Sherr, B. F., E. B. Sherr, and J. McDaniel.** 1992. Effect of protistan grazing on the frequency of dividing cells in bacterioplankton assemblages. Appl. Environ. Microbiol. **58:**2381–2385.
28a. **Sieracki, M. E.** Personal communication.
29. **Sieracki, M. E., P. W. Johnson, and J. M. Sieburth.** 1985. Detection, enumeration, and sizing of planktonic bacteria by image-analyzed epifluorescence microscopy. Appl. Environ. Microbiol. **49:**799–810.
30. **Sieracki, M. E., S. E. Reichenbach, and K. L. Webb.** 1989. Evaluation of automated threshold selection methods for accurately sizing microscopic fluorescent cells by image analysis. Appl. Environ. Microbiol. **55:**2762–2772.
31. **Viles, C. L., and M. E. Sieracki.** 1992. Measurement of marine picoplankton cell size by using a cooled, charge-coupled device camera with image-analyzed fluorescence microscopy. Appl. Environ. Microbiol. **58:**584–592.
32. **Zwart, K. B., J. Bloem, L. A. Bouwman, L. Brussaard, W. A. M. Didden, G. Lebbink, J. C. Y. Marinissen, M. J. Vreeken-Buijs, S. L. G. E. Burgers, and P. C. de Ruiter.** 1994. Population dynamics in the belowground food webs in two different agricultural systems. Agric. Ecosyst. Environ. **51:**187–198.

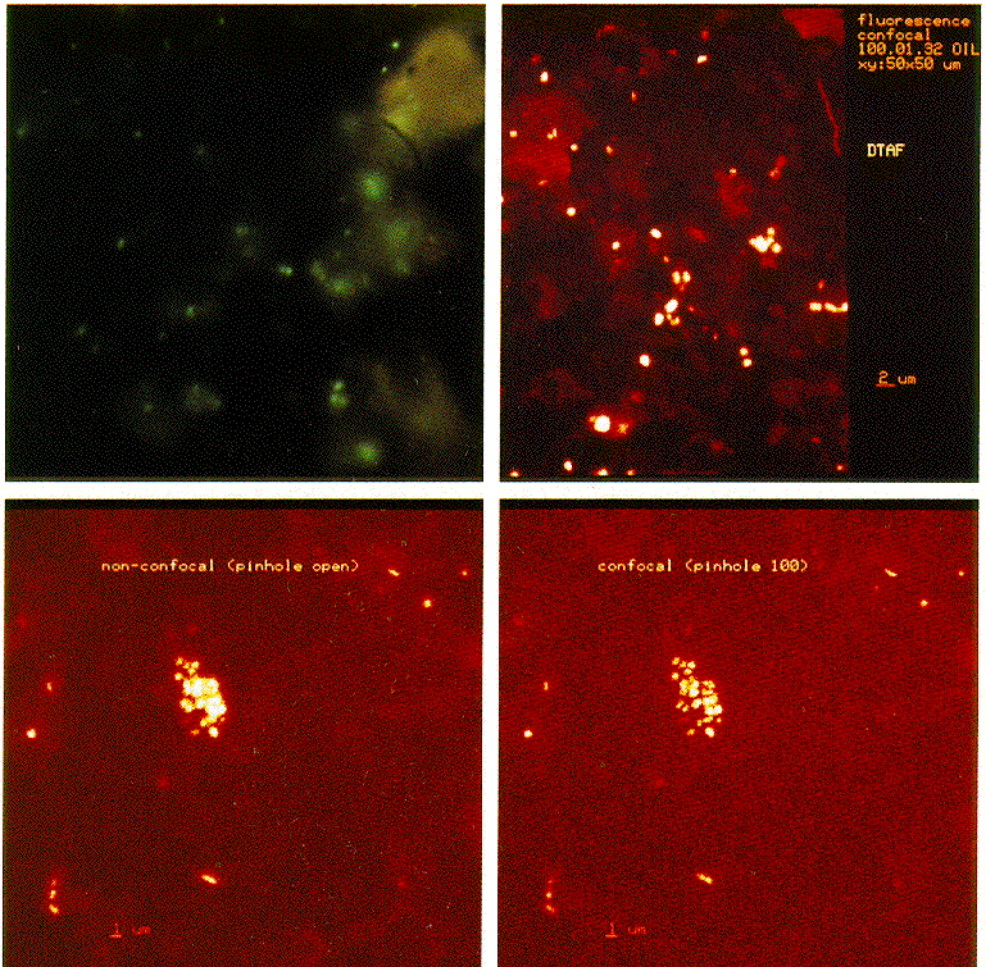
a
fluorescence
confocal
100.01.32 OIL
xy:50x50 um
DTAF
2 um
b
non-confocal (pinhole open)
1 um
c
confocal (pinhole 100)
1 um
d

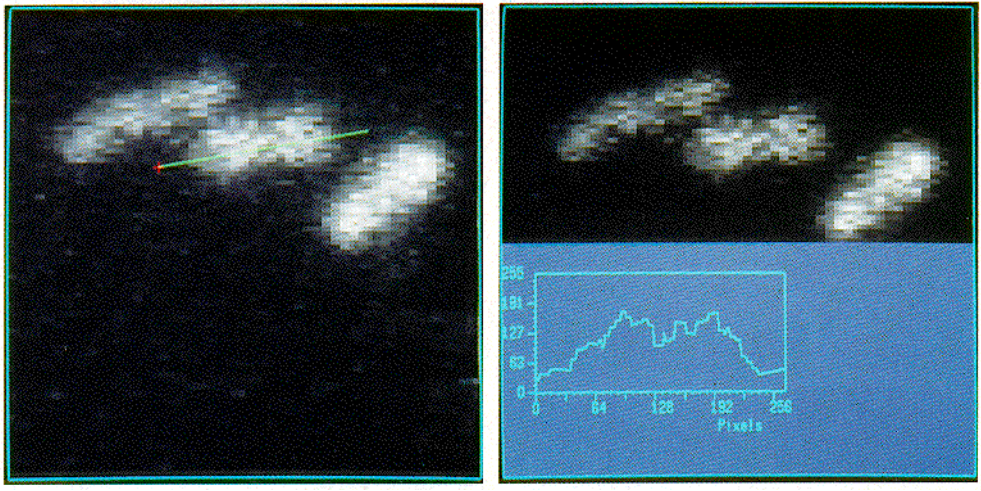

a

b

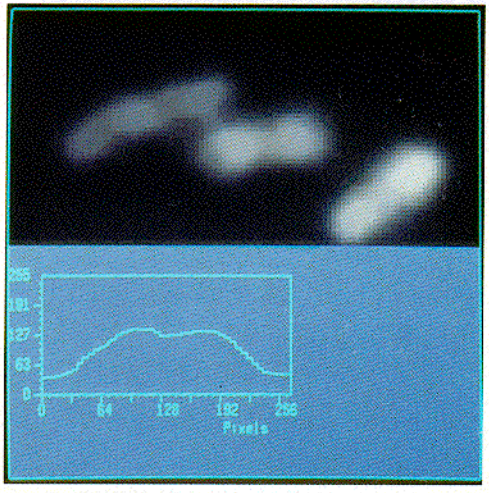
255
191
127
63
0
0
64
128
192
255
Pixels

c

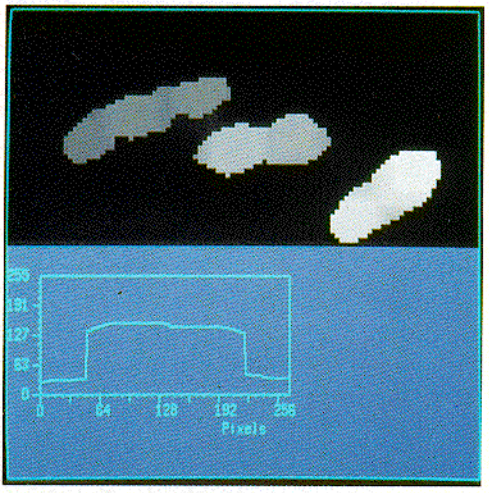
255
191
127
63
0
0
64
128
192
255
Pixels

d

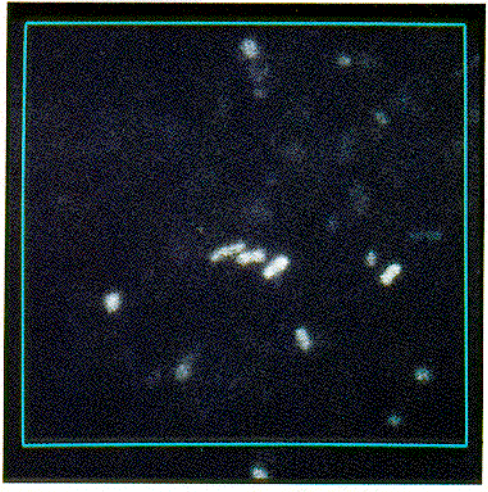

e

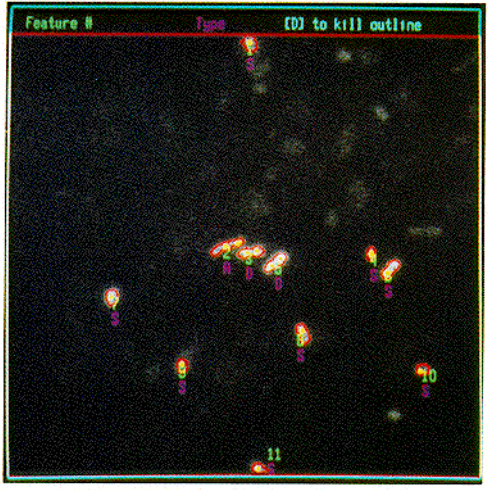

f

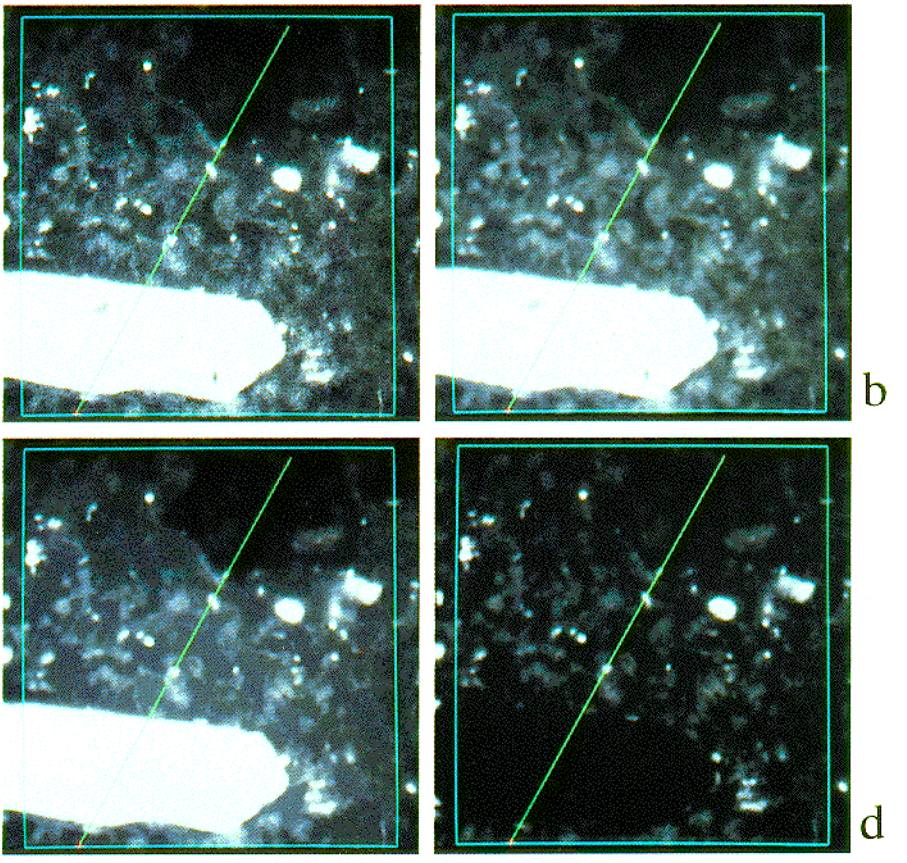
a
b
c
d

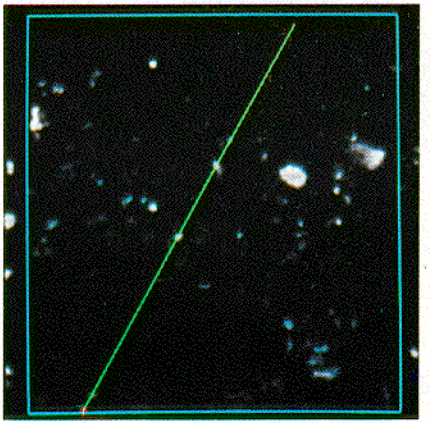

e

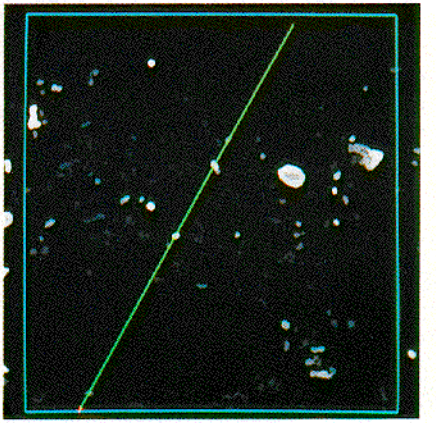

f

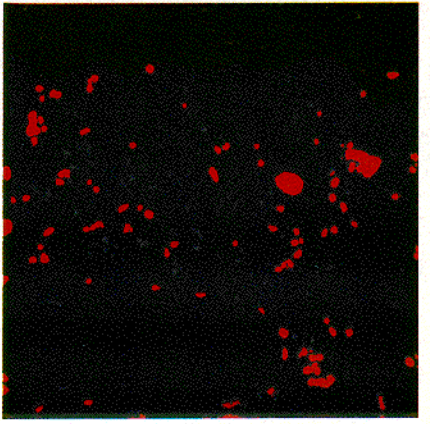

g

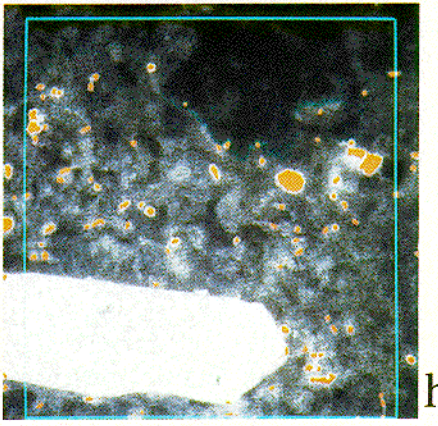

h